

1
2 **The Improvement to the Environment Wind and Tropical Cyclone Circu-**
3 **lation Retrievals with Modified GBVTD (MGBVTD) Technique**
4

5
6 Xiaomin Chen, Kun Zhao *

7 Key Laboratory for Mesoscale Severe Weather/MOE and School of Atmospheric Science,
8 Nanjing University, Nanjing, China
9

10 Wen-Chau Lee

11 National Center for Atmospheric Research, Boulder, Colorado
12

13 Ben Jong-Dao Jou

14 Department of Atmospheric Sciences, National Taiwan University, Taipei, Taiwan
15

16 Ming Xue

17 Center for Analysis and Prediction of Storms, and School of Meteorology, University of Ok-
18 lahoma, Norman, Oklahoma, 73072
19

20 Paul R. Harasti

21 U.S. Naval Research Laboratory, Monterey, California
22

23 January, 2013
24

25 Submitted to Journal of Applied Meteorology and Climatology
26

27 Accepted May 2013
28

* *Corresponding author address:* Kun Zhao, Key Laboratory of Mesoscale Severe Weather/MOE, School of Atmospheric Sciences, Nanjing University, 22 Hankou Road, Nanjing, P.R. China, 210093.
E-mail: zhaokun@nju.edu.cn

29
30
31
32
33
34
35
36
37
38
39
40
41
42
43
44
45
46
47
48
49
50
51
52
53

Abstract

The Ground-based Velocity Track Display (GBVTD) was developed to deduce three-dimensional primary circulation of landfalling tropical cyclones (TCs) from a single-Doppler radar data. However, its intrinsic closure assumptions prevent the cross-beam component of the mean wind (V_M) be resolved and consequently aliased into the retrieved axisymmetric tangential wind (V_{T0}). Recently, the development of the hurricane volume velocity processing method (HVVP) enabled independent estimate of V_M , but its accuracy is limited by a suite of empirical assumptions to deduce the modified Rankine-combined vortex exponent (X_T). By combing GBVTD with HVVP techniques, this study proposes a modified GBVTD method (MGBVTD) to objectively deduce X_T from the GBVTD technique and provide a more accurate estimation of V_M and V_{T0} .

MGBVTD retains the strength in both algorithms but avoids their weakness. The GBVTD-retrieved TC circulation can be used to anchor the TC wind profile for HVVP to deduce $V_{M\perp}$ and then be included in the GBVTD analysis to reduce the biases in the retrieved TC circulation. A better TC circulation can be obtained via an iterative process in MGBVTD. The results from idealized experiments demonstrate that the MGBVTD-retrieved cross-beam component of V_M are within 2 m s^{-1} of reality. We applied MGBVTD to Hurricane Bret (1999) whose inner core was captured simultaneously by two WSR-88D radars. The MGBVTD-retrieved cross-beam component of V_M from single-Doppler radar data are very close to that from Dual-Doppler radar synthesis using Extended GBVTD (EGBVTD) with their difference less than 2 m s^{-1} . The mean difference in the MGBVTD-retrieved V_{T0} from the two radars is $\sim 2 \text{ m s}^{-1}$, significantly smaller than that resolved in GBVTD retrievals ($\sim 5 \text{ m s}^{-1}$). Finally, the limitation of MGBVTD is discussed.

1. Introduction

Landfalling tropical cyclone (TC) is one of the most devastating and deadly natural disasters along coastal regions of many countries. Accurately monitoring inner core structure and its evolution before and after landfall is crucial for the protection of life and property. Doppler weather radar is the only platform that can capture the three-dimensional (3D) structure of landfalling TCs with high spatial ($\sim 1 \text{ km}$) and temporal ($\sim 6 \text{ min}$) resolutions. Donaldson (1970) found that a vortex produces a Doppler velocity dipole signature with opposite parity in a plan position indicator (PPI) mode. Based on the location and magnitude of this Doppler velocity dipole, Wood and Brown (1992) developed a pattern-recognition algorithm to estimate the three critical characteristics of vortex structure, including the center, the radius of maximum wind (R_{max}) and the maximum wind speed. However, this method cannot quantitatively provide the detailed 3D circulation of a TC.

Lee et al. (1994) proposed a robust single-Doppler wind retrieval technique, called the Velocity Track Display (VTD), to deduce the primary circulations of TCs at different altitudes in real time from an airborne tail Doppler radar on board the National Oceanic Atmospheric Administration WP-3D aircraft. In order to study the landfalling TCs using coastal radars, Lee et al. (1999) reformulated the VTD equations for a ground-based Doppler radar, called ground-based VTD (GBVTD). Recently, successful applications of GBVTD to several landfalling TCs (Lee et al. 2000, Lee and Bell 2007, Zhao et al. 2008) have demonstrated its ability in monitoring and warning. A series of GBVTD extensions including, Ground-based Extended VTD (GB-EVTD, Roux et al. 2004), Extended GBVTD (EGBVTD, Liou et al.

2006), Generalized VTD (GVTD, Jou et al. 2008) and Gradient VTD (GrVTD, Wang et al. 2012), expanded the GBVTD analysis into multiple flight legs for airborne Doppler radar, multiple ground-based Doppler radars and direct use of aliased radial velocity data, etc. However, the cross-beam component of the mean wind ($V_{M\perp}$) is neglected in all of the aforementioned VTD-family of technique and is consequently aliased into the retrieved axisymmetric tangential wind (V_{T0}).

Several methods have been developed to estimate the $V_{M\perp}$ independently, including the hurricane volume velocity processing method (HVVP, Harasti et al. 2003), using the storm motion as a proxy of mean wind (Harasti et al. 2004), extended-HVVP method (EHVVP, Zhu et al. 2010) and the extended-GBVTD method (EGBVTD, Liou et al. 2006). Among these existing methods, the use of storm motion as a proxy is the easiest to implement, but it assumes that the mean wind vectors are not a function of height which is not realistic. The EGBVTD technique can provide a relatively accurate estimation of $V_{M\perp}$, but requires dual- or multiple-Doppler radar observations of TCs that are rarely available due to the typically large baseline between operational Doppler radars. In comparison, HVVP is attractive because it estimates $V_{M\perp}$ at different altitudes using only single Doppler radar data and an empirical modified-Rankine tangential wind profile (hereafter, refer as Rankine profile). The successful applications of HVVP to several real TCs (Harasti et al. 2003) have shown its potential for the operational use. Recently, HVVP has been successfully incorporated, together with GBVTD, into the Vortex Objective Radar Tracking and Circulation (VORTRAC) software for real-time analysis of TCs at the National Hurricane Center (NHC) of the United States. Despite these encouraging results, the HVVP technique is limited by its fundamental assumption, the modified Rankine-combined vortex exponent (X_T), required to separate $V_{M\perp}$ from the TC circulations using empirical equations. Hence, the HVVP-retrieved $V_{M\perp}$ may contain large uncertainties resulting from the deviation of the HVVP-estimated and the true X_T . Furthermore, in contrast to recently developed EHVVP technique (Zhu et al. 2010) that assumes a Rankine-combined vortex in the analytical experiments, the major advantage of MGBVTD over EHVVP is the use of a modified Rankine-combined vortex.

In this paper, an improved method, named Modified GBVTD (MGBVTD) is proposed to retrieve the TC mean wind vectors and the primary circulations simultaneously by combining the strength of the HVVP and GBVTD to yield a more realistic TC circulation. Section 2 describes the mathematical formulations and details of MGBVTD. A series of analytical datasets based on a modified Rankine-combined vortex are employed to evaluate the performance of MGBVTD technique in different situations in Section 3. In Section 4, the MGBVTD is applied to Hurricane Bret (1999) observed simultaneously by two coastal WSR-88D Doppler radars and its retrieved winds are compared with those deduced by EGBVTD. Summary and discussion are given in section 5.

2. The MGBVTD method

As MGBVTD combines GBVTD and HVVP, these two methods are summarized below. For simplicity, a unified coordinate system is employed on both methods to make the description more consistent.

a) GBVTD

Only a brief explanation of the original GBVTD formulations is given in this section. Interested reader can refer to Lee et al. (1999) for more details. The same symbols and geome-

try relationships as in Lee et al. (1999) are adopted in this article except for the TC center is located to the north of the radar (as shown in Fig.1).

The GBVTD method is proposed to provide an estimate of the horizontal winds of TC circulation relative to the mean wind vector (V_M) around rings concentric with the circulation center. The mean wind is considered as environmental wind which only varies with height across the inner core of a TC. For the convenience of later discussions, V_M consists two components, the along beam component ($V_{M\parallel}$) and the cross-beam component ($V_{M\perp}$), with respect to the north that passes through the circulation center. Least-squares curve fitting of the observed Doppler velocity data are performed around the GBVTD rings and the resulting Fourier coefficients can be bridged to various wavenumber components of tangential and radial winds, including $V_{M\parallel}$. There are many ways to interpret GBVTD solutions since the set of equations is not closed. Lee et al. (1999) proposed the closure assumption in which the asymmetric radial wind is negligible when compared with the corresponding tangential wind. In addition, the maximum wavenumber resolved at each radius varies with the maximum angular data gap; for data having gaps of 30° , 60° , 120° , and 180° , the maximum wavenumbers resolved are 3, 2, 1, and 0, respectively.

GBVTD can only provide an estimation of $V_{M\parallel}$ while the unresolved $V_{M\perp}$ is aliased into the axisymmetric tangential wind as described in (20) in Lee et al. (1999):

$$V_{T0} = -B_1 - B_3 - V_M \sin(\theta_T - \theta_M) \times \sin \alpha_{\max} + V_R S_2, \quad (1)$$

where B_1 and B_3 are the Fourier coefficients of GBVTD analysis at a given radius (note that the typo error of the sign before B_3 in Lee et al. (1999) has been corrected), θ_T and θ_M are the angles for the circulation center relative to the radar and the direction of the mean wind, respectively. $V_M \sin(\theta_T - \theta_M)$ is $V_{M\perp}$ and $\sin \alpha_{\max} = R / R_T$, where R (R_T) is the range from the circulation center to the GBVTD ring (radar). The last term on the right-hand side of (1) was ignored in the original formulation of GBVTD and it is aliased into V_{T0} .

b) HVVP

Harasti et al. (2003) proposed the Hurricane Volume Velocity Processing (HVVP) method to provide an estimate of the mean wind vectors of a TC as a function of height. In contrast to GBVTD, HVVP assumes a modified Rankine-combined vortex model in which the tangential wind profile outside the vortex inner core could be described in (2) - (3) while inner core exhibits solid body rotation. The radial wind profile outside the vortex inner core is also shown in Eqs. (4)-(5).

$$V_{T0}(R, z) = V_{T0}(R_T, z) [R_T / R]^{X_T}, \quad (2)$$

$$V_T(R_T, z) = \left[1 + \sum_n A_n \cos n(\gamma - \delta_n) \right] V_{T0}(R_T, z), \quad (3)$$

$$V_{R0}(R, z) = V_{R0}(R_T, z) [R_T / R]^{X_R}, \quad (4)$$

$$V_R(R_T, z) = \left[1 + \sum_n \lambda_n \cos n(\gamma - \sigma_n) \right] V_{R0}(R_T, z), \quad (5)$$

n represents the wavenumber ($n = 1, 2, 3$), and A_n (δ_n) is the magnitude (phase) of the asymmetric tangential wind for angular wavenumber n . Similarly, for asymmetric radial wind

the magnitude (phase) is $\lambda_n(\sigma_n)$. $V_T(R_T, z)$ ($V_R(R_T, z)$) is tangential (radial) wind at z altitude over the radar site, including the axisymmetric and asymmetric components. Then HVVP uses the tangential and radial wind information expressed in (2)-(5) over the radar site to retrieve $V_{M\perp}$ and $V_{M\parallel}$ at different altitudes. Donaldson et al. (1991) proposed a simple technique to estimate kinematic properties of a wind field of a Hurricane based on the modified Rankine-combined vortex assumption in which the shearing deformation of the wind field can be expressed as:

$$\text{shearing deformation} = (1 + X_T)V_T(R, z) / R, \quad (6)$$

HVVP assumes the observed Doppler velocity (V_d) is equal to the sum of the estimated Doppler velocity and the measurement error ε . It connects the estimated coefficient of a second-order Taylor series expansion of the wind field to the kinematic properties of the analytic datasets in a three-dimension volume. The shearing deformation term shown in (6) as K_7 can be calculated:

$$\left. \begin{aligned} V_d &= \sum_{m=1}^{16} P_m^T K_m + \varepsilon \\ P_1 &= -\cos \varphi \sin \alpha, & K_1 &= u_0, \\ P_2 &= r \cos^2 \varphi \sin^2 \alpha, & K_2 &= u_x, \\ P_3 &= -\cos \varphi \sin \alpha (z - z_0), & K_3 &= u_z, \\ P_4 &= \cos \varphi \cos \alpha, & K_4 &= v_0, \\ P_5 &= r \cos^2 \varphi \cos^2 \alpha, & K_5 &= v_y, \\ P_6 &= \cos \varphi \cos \alpha (z - z_0), & K_6 &= v_z, \\ P_7 &= -r \cos^2 \varphi \sin \alpha \cos \alpha, & K_7 &= u_y + v_x, \\ P_8 &= -r^2 \cos^3 \varphi \sin^3 \alpha, & K_8 &= u_{xx} / 2, \\ P_9 &= -r^2 \cos^3 \varphi \sin \alpha \cos^2 \alpha, & K_9 &= v_{xy} + u_{yy} / 2, \\ P_{10} &= r^2 \cos^3 \varphi \cos^3 \alpha, & K_{10} &= v_{yy} / 2, \\ P_{11} &= r^2 \cos^3 \varphi \cos \alpha \sin^2 \alpha, & K_{11} &= u_{xy} + v_{xx} / 2, \\ P_{12} &= r \cos^2 \varphi \sin^2 \alpha (z - z_0), & K_{12} &= u_{xz}, \\ P_{13} &= r \cos^2 \varphi \cos^2 \alpha (z - z_0), & K_{13} &= v_{yz}, \\ P_{14} &= -r \cos^2 \varphi \sin \alpha \cos \alpha (z - z_0), & K_{14} &= u_{yz} + v_{xz}, \\ P_{15} &= -\cos \varphi \sin \alpha (z - z_0)^2, & K_{15} &= u_{zz}, \\ P_{16} &= \cos \varphi \cos \alpha (z - z_0)^2 \quad \text{and} & K_{16} &= v_{zz}, \end{aligned} \right\} \quad (7)$$

where P_m is the coefficient matrix, K_m are the predicted parameters which can be solved by the least squares curve-fitting. HVVP uses a spherical coordinate $(r, 360-\alpha, \varphi)$ where the elevation angle of the radar beam and altitude at each V_d datum are φ and z , respectively. Here, α is the angle adapted from GBVTD coordinate which is measured counterclockwise from the radar beam passing through TC center to the data position on a GBVTD ring. z_0 represents the altitude of analysis and u_0 (v_0) is the total wind component in the cross-beam (along-beam) direction at z_0 altitude.

The tangential and radial wind over the radar site can be calculated from retrieved K_7 and K_2 :

$$V_T(R_T, z) = R_T K_7 / [1 + X_T], \quad (8)$$

$$V_R(R_T, z) = R_T K_2 \quad (9)$$

so $(V_{M\perp}, V_{M\parallel})$ can be computed:

$$V_{M\perp}(z) = u_0 - V_T(R_T, z). \quad (10)$$

$$V_{M\parallel}(z) = v_0 + V_R(R_T, z). \quad (11)$$

To accurately separate the mean wind, it is imperative to retrieve the TC circulation as close as possible to the truth. However, the HVVP method still encounters one major problem. The X_T in (8) is calculated using the following empirical equation that is derived from a simplification to the axisymmetric tangential momentum equation (2.11) in Willoughby (1995),

$$X_T = \begin{cases} X_R / 2 & X_R > 0, V_R < 0 \\ 1 - X_R & X_R < 0, V_R < 0 \end{cases}; \quad (12)$$

where $X_R = -K_5 / K_2$. As Harasti (2003) suggests the simplifying assumptions in (12) may not be always valid for different TCs, and thus result in the errors in the estimated mean wind. A possible solution is to use the GBVTD-derived $V_{M\parallel}$ to replace HVVP-derived $V_{M\parallel}$ and reduce the bias in $V_{M\perp}$ when the asymmetric radial winds are small.

c) Modified GBVTD (MGBVTD) method

To reduce the error in estimating the $V_{M\perp}$ caused by using an empirical X_T in HVVP, MGBVTD method is developed by combining the merits of GBVTD and HVVP methods.

In this framework, the axisymmetric tangential wind V_{T0} and asymmetric TC circulations can be typically expressed as Eqs. (2) and (3). In GBVTD, the V_{T0} at different radii can be retrieved rather accurately if a guessed $V_{M\perp}$ ($V_{M\perp,guess}$) is provided. Given the radial profile of V_{T0} , the parameter X_T in (2) can be objectively determined by fitting the GBVTD-derived V_{T0} profile. By substituting this X_T into HVVP, a more accurate $V_{M\perp}$ ($V_{M\perp,ret}$) can be retrieved. If $V_{M\perp,guess}$ converges to $V_{M\perp,ret}$, $V_{M\perp,guess}$ is considered the "true" $V_{M\perp}$. Therefore, it is able to search for the "optimal" $V_{M\perp}$ by examining a reasonable range of $V_{M\perp,guess}$.

The procedure of MGBVTD is described as follows. In this study, the magnitude of guessed $V_{M\perp}$ varies from -20 to 20 m s⁻¹ with increments of 0.1 m s⁻¹. In the first step, for an individual $V_{M\perp,guess}$, the axisymmetric tangential wind profile can be computed by GBVTD with the correction of $V_{M\perp,guess}$ in (1). Based on the GBVTD-retrieved V_{T0} profile, X_T can be calculated by minimizing the objective function $f1$ derived by taking logarithm of (2):

$$f1 = \sum_{i=N1}^{N2} [\log V_{T0}(R_T) + X_T \log[R_T / i] - \log(V_{T0}(i))]^2 = \min, \quad (13)$$

where i denotes the i^{th} radius whose magnitude is from the $N1$ to $N2$ km. In our test, $N1$ is set as R_{\max} and $N2$ is usually about 70% of R_T to ensure sufficient fitting samples.

In the second step, by substituting X_T into (7), (8) and (10), the HVVP-retrieved $V_{M\perp,ret}$ can be obtained.

Finally, the difference between $V_{M\perp guess}$ and $V_{M\perp ret}$ can be calculated as:

$$f2 = 10 \log(V_{M\perp guess} - V_{M\perp ret}) = \min . \quad (14)$$

Note that the reason why taking the logarithm form is simply to amplify the anomaly. Repeating the first and second steps for all the guessed $V_{M\perp guess}$ within the given range and the $V_{M\perp guess}$ is considered as the "optimal" $V_{M\perp}$ when $f2$ reaches its minimum. Combining the "optimal" $V_{M\perp}$ and $V_{M\parallel}$ provided by GBVTD, MGBVTD method provides a more accurate estimate of mean wind without those extensive empirical assumptions required in the HVVP and hence improves the accuracy of GBVTD-derived axisymmetric tangential winds.

3. Tests using analytic data

a) Construction of analytic dataset

To quantitatively investigate the performance of the MGBVTD method, a set of idealized vortex flow fields, based on a single-layer (elevation angle φ equals 0) modified Rankine-combined vortex, is constructed to simulate V_d , following Lee et al. (1999). The mathematical expressions for the axisymmetric tangential wind (V_{T0}) and radial wind (V_{R0}) are

$$V_{T0} = V_{\max} \left(\frac{R}{R_{\max}} \right), R \leq R_{\max} ,$$

$$V_{T0} = V_{\max} \left(\frac{R_{\max}}{R} \right)^{x_T}, R > R_{\max} , \quad (15)$$

$$V_{R0} = C_1 [(R_{\max} - R)R]^{1/2}, R \leq R_{\max}$$

$$V_{R0} = -C_2 (R - R_{\max})^{1/2} R_{\max} / R, R > R_{\max} , \quad (16)$$

where V_{\max} and R_{\max} are set to 50 m s⁻¹ and 20 km, respectively. C_1 and C_2 are scale factors and are assigned 0.1 s⁻¹ and 3 m^{0.5} s⁻¹, respectively. Apparently, the outflow (inflow) is inside (outside) R_{\max} according to Eq. (17). The asymmetric tangential wind follows Eq. (3) where A_n ($n=1, 2, 3$) is the magnitude of each wavenumber and is set to 0.2. Following Lee et al. (1999), there is no asymmetric radial component in the idealized vortex.

A hypothetical Doppler radar is located at the grid origin (0, 0) with a maximum effective range of 150 km and a high effective Doppler velocity where velocity aliasing is not considered. The TC center is set at 80 km north of the radar site at (0, 80). The TC circulation generated by (3), (15) and (16) is projected onto the radar beam direction to produce analytic V_d . The mean wind speed (V_M) and direction (θ_M) are arbitrarily assigned to 10 m s⁻¹ and 0~360°. When the θ_M is set as 180° (easterly), there is only $V_{M\perp}$ information. The analytic V_d data are used to retrieve the total winds of TCs using GBVTD and MGBVTD for comparison against the analytic modified Rankine-combined vortex. As a quantitative measure of the accuracy of GBVTD and MGBVTD retrievals, the root mean square error (RMSE) of the total winds between retrieved and the true values are calculated as

$$RMSE = \sqrt{\frac{\sum_{i=1}^N (V - V_{ref})^2}{N}} . \quad (17)$$

Here V and V_{ref} are the quantities to be verified and true value, respectively. N indicates the total number of data points of the valid values. Besides, the correlation coefficient (CC) between the retrieved and true value is calculated in the idealized experiments.

b) Results of retrieved MGBVTD winds

A series of experiments was designed to examine the performance of MGBVTD-retrieved mean wind in the presence of 1) different direction of V_M , 2) different X_T , 3) various R_{\max} , 4) tangential wind asymmetry and 5) a misplaced center. A description of these experiments is given in Table 1. Without specific description, V_d is generated from the same idealized axisymmetric vortex with $V_{\max} = 50 \text{ m s}^{-1}$, $R_{\max} = 20 \text{ km}$ and $X_T = 1.0$ using (13) and (14). In this study, the TC center is defined as the circulation center and its location is known for the analytical series.

1) Sensitivity to the direction of V_M (GM1)

To examine the impact of different direction of mean wind on MGBVTD method, GM1 is conducted in which V_M equals 10 m s^{-1} while θ_M varies from 0° to 360° . The retrieved V_M and θ_M are nearly identical to their true counterparts (Fig. 2a). The magnitude of retrieved mean wind is within 0.1 m s^{-1} to its true value in every run and the diagonal line of retrieved direction of mean wind indicates the error is negligible. Thus it is concluded that MGBVTD is insensitive to the direction of mean wind.

To better understand the searching process of $V_{M\perp}$ for MGBVTD, an example (Fig. 2b) is given when θ_M equals 180° and $|V_{M\perp}| = 10.0 \text{ m s}^{-1}$. The search range of $V_{M\perp, \text{guess}}$ is set from -20 m s^{-1} to 15 m s^{-1} . When $V_{M\perp, \text{guess}}$ equals the true $V_{M\perp}$ (-10.0), the fitting error f^2 reaches its minimum (near -30.0) and the retrieved X_T is treated as the true value of the Rankine profile. The corresponding GBVTD- and MGBVTD-retrieved total winds (axisymmetric tangential and radial winds plus a mean wind) are shown in Fig. 3b and Fig. 3c, as compared with the analytic wind in Fig. 3a. Clearly, we see better agreement between the MGBVTD-retrieved magnitudes in Fig. 3c and the analytical wind magnitudes in Fig. 3a. Despite a slight underestimation of the total wind in the south part of the TC at $\sim 20 \text{ km}$ radius, the general wind pattern (Fig. 3c) indicates a coherent wavenumber-1 pattern with similar magnitude and phase to the analytical wind field (Fig. 3a), which is consistent with the characteristics of the Rankine-combined vortex with an easterly mean wind as shown in Fig.5 of Lee et al. (1999). On the contrary, as GBVTD cannot retrieve the cross-beam component of mean wind, there is no wavenumber-1 signal in the wind pattern retrieved by GBVTD (Fig. 3b). The corresponding error statistics, RMSE (CC) of GBVTD- and MGBVTD- retrieved total wind field, are 8.5 m s^{-1} (0.82) and 0.2 m s^{-1} (1.0), respectively (not shown), which quantitatively proves that MGBVTD can retrieve a more accurate wind field than GBVTD with the presence of $V_{M\perp}$.

For further inspection, GBVTD- and MGBVTD-retrieved axisymmetric tangential wind profiles are shown as gray lines in Fig. 3d. Compared to the Rankine profile (black solid line), the GBVTD retrieval is underestimated. The discrepancy between them becomes larger at farther radii, which can be easily understood since more $V_{M\perp}$ is aliased into mean tangential wind when $\sin \alpha_{\max}$ is larger as shown in (1). Whereas, MGBVTD performs very well due to its ability to retrieve $V_{M\perp}$, as indicated by the overlap between its retrieved profile (gray dash line) and Rankine profile.

2) Sensitivity to Rankine X_T (GM2)

The multi-storm statistical study of Gray and Shea (1973) indicates that the mean value found for X_T was 0.5 and was close to the expected theoretical value, but with relatively large standard deviations (0.3). It is believed that the stage of TC life cycle accounts for much of the variability in the tangential wind profile shape (e.g., Weatherford 1989). Considering the fact, the testing range for X_T is set from 0.3 to 1.0 in GM2 run. The larger X_T is, the faster the profile drops down with radius. A dimensionless parameter Par is introduced and is defined as:

$$Par = R_a / (R_T - R_{max}), \quad (18)$$

where R_a represents the radius of HVVP analysis domain centered at the radar. When the HVVP analysis domain extends to R_{max} , $Par = 1.0$. The lower bound of Par is set to 0.3 in this sensitivity test to ensure enough data points for analysis. The upper bound of Par is set to 0.7 as larger value of Par tends to cause large estimation error of the deformation term of HVVP (K_7), thus degrading the retrieved $V_{M\perp}$. For diverse X_T and Par , RMSE of the retrieved axisymmetric tangential wind profile to their true counterparts is computed (Fig. 4a). It is evident (Fig. 4a) that RMSE is proportional to Par with the same X_T while RMSE is inversely proportional to X_T with fixed Par . The similar correlation can be inferred with the retrieved $V_{M\perp}$ (Fig. 4b). The largest error of the retrieved $V_{M\perp}$ is $\sim 1.3 \text{ m s}^{-1}$ to the true value when $X_T = 0.3$ and $Par = 0.7$. To quantitatively measure the variation of the retrieved $V_{M\perp}$ for different Par , the standard deviation (STD) for all X_T are shown in Table 4. The maximum STD of 0.4 occurs when $X_T = 0.3$, which is consistent with the large space between the five lines shown in Fig. 4b. However, the low values for both the RMSE of the retrieved V_{T0} profile ($< 0.3 \text{ m s}^{-1}$) and the STD of $V_{M\perp}$ indicate MGBVTD can reliably retrieve V_M and the TC primary circulations on a wide range of wind profiles (i.e., X_T). To illustrate the advantage of MGBVTD over HVVP in the estimation of TC winds, the retrieved X_T and $V_{M\perp}$ using HVVP are shown in Fig. 4c and Fig. 4d. Apparently, the estimated X_T from HVVP are nearly constant despite the variation of the true X_T due to the application of empirical equation (13), thus leading to a larger error in the estimate of $V_{M\perp}$ (more than 9 m s^{-1} when $X_T > 0.7$).

Note that HVVP is not expected to perform well with a radial wind model such as (16) since it is not related to the expected radial wind profile derived from the axisymmetric momentum equation from which (15) result. The other tests using V_R model proposed in HVVP (i.e. Eq. (4)) are also performed. However, even in this situation, HVVP can only retrieve a comparable result to MGBVTD when inflow exists outside R_{max} and $X_T = X_R / 2$ (not shown), which is reasonable since it is exactly the empirical equation in (12). This fact supports MGBVTD could be applied more generally.

3) Sensitivity to R_{max} (GM3)

As the size of TC's eye changes considerably from case to case, it is indispensable to test the performance of MGBVTD to TCs with different R_{max} . A dimensionless parameter ρ is introduced as $\rho = R_{max} / R_T$. The errors for the retrieved X_T and $V_{M\perp}$ shown in Fig. 5 remain considerably small generally but become larger when ρ is greater than 0.5 (i.e., the radar is within twice the R_{max} of the TC center). When the RMW approaches a radar, there are fewer

radii available for the GBVTD analysis to deduce X_T leading to a less stable fitting of the radial wind profile. However, even in this situation, the largest retrieved error of $V_{M\perp}$ (X_T) is 0.2 m s^{-1} (0.01) that can be essentially neglected.

4) Sensitivity to asymmetry (AV SERIES)

Based on GM1 to GM3 tests aforementioned, three experiments are conducted to examine the impact of asymmetric circulation, including wavenumber one, two and three (AV1, AV2 and AV3) embedded within the axisymmetric vortex plus a mean flow. The asymmetric structure is generated using Eq. (3) and the parameters are listed in the Table 3.

The retrieved X_T ($V_{M\perp}$) in all AV series oscillate in a wavelike behavior around the true value consistent with the corresponding asymmetric structures (i.e., wavenumbers) (Fig. 6a, 6b). The retrieved errors of X_T ($V_{M\perp}$) are less than 0.05 (0.5 m s^{-1}) in AV1-AV3 experiments where the errors are less than 5% of the specified values. The performances of GBVTD and MGBVTD for asymmetric TCs are compared in all AV1-AV3 experiments (Fig. 7). Similar to that in Fig. 2c, the GBVTD cannot accurately deduce total wind structure in AV1-AV3 tests which is mainly due to the inability of GBVTD to retrieve $V_{M\perp}$. In comparison, MGBVTD can reproduce all major features of the wavenumber 1-3 structures well, especially the amplitude and phase of asymmetry. Nevertheless, the retrieved total winds of MGBVTD do suffer pronounced distortion in higher wavenumber asymmetry similar to that of GBVTD. For example, the peak amplitude of wavenumber 3 is significantly reduced on the far side of the TC in both Figs. 7b3 and 7c3, even though MGBVTD has contained the $V_{M\perp}$ information. This is mainly due to the geometric distortion inherent in GBVTD non-linear coordinate, consistent to the description in Lee et al. (1999). The corresponding error statistics (Fig. 8) show that the experiments with asymmetric tangential wind component tend to have slightly larger errors than that of GM1~3, especially for higher wavenumbers. The RMSEs of GBVTD- (MGBVTD-) retrieved total winds in AV1-AV3 experiment are 8.8 (0.2) m s^{-1} , 8.4 (0.7) m s^{-1} , 10.6 (3.2) m s^{-1} , respectively. The MGBVTD-retrieved total winds in AV1-AV3 experiments also show higher value of CCs (Fig. 8). The main reason for the large RMSE errors and the relatively low CCs in the GBVTD retrieved total wind is its inability to retrieve $V_{M\perp}$ at 10 m s^{-1} amplitude. In contrast, MGBVTD can retrieve accurate $V_{M\perp}$ and is also quite robust when the TC circulation is asymmetric.

In contrast to the asymmetric tangential winds, the asymmetric radial winds radial winds cannot be resolved in MGBVTD frame. When significant asymmetric wavenumber 2 components of V_R ($V_R S_2$) exist as shown in Eq. (1), the estimated axisymmetric tangential wind and X_T may contain large error, and thus lead to the bias in the estimate of $V_{M\perp}$. In this situation, some extra wind measurements are required to retrieve the asymmetric radial flow (Liou et al., 2006), which is beyond the scope of this paper.

5) A misplaced center (GC)

Previous studies (e.g., Roux and Marks 1996; Lee and Marks 2000) have shown the quality of GBVTD-retrieved winds is sensitive to the center uncertainties. Lee and Marks (2000) noted that a 5-km deviation of the TC center can produces 20% error of GBVTD-retrieved axisymmetric tangential component. To examine the impact of the center uncertainty on MGBVTD retrievals, we calculated the errors of the MGBVTD-retrieved X_T and $V_{M\perp}$ for various center displacements. As shown in Fig.9, the error is proportional to the center displacement, and the error is more sensitive to the center displacement in X-axis (perpendic-

ular to the beam through the TC center) than that in Y-Axis. In general, MGBVTD perform very well when the misplaced center is within 3 km, and the maximum error of the retrieved X_T ($V_{M\perp}$) is about 0.08 (1 m s^{-1}). Lee and Marks (2000) developed a ‘‘Simplex’’ algorithm, which can estimate the TC center within 0.34 km (2 km) of the true center for analytical (real) TCs. This suggests that MGBVTD has an ability to retrieve accurate $V_{M\perp}$ for a real TC by using the GBVTD-Simplex-estimated TC center.

4. Testing of MGBVTD with Hurricane Bret

In this section, Hurricane Bret (1999) is selected to test the performance of MGBVTD. Bret was a category 4 hurricane before it weakened to a category 3 hurricane a few hours before landfall along the coast of Texas. Two WSR-88D coastal radars located at Corpus Christi (KCRP) and Brownsville (KBRO) made simultaneous observations as Bret made landfall midway between them.

A constant-altitude PPI (CAPPI) mosaic of reflectivity from KCRP and KBRO at 0000 UTC August 23 1999 is shown in Fig. 10a indicating KCRP was located in a region of mostly convective precipitation while KBRO was located in a region of mostly stratiform precipitation. The corresponding 2 km CAPPI image of Doppler velocity from KCRP at 2357 UTC (KBRO at 0000 UTC) is illustrated in Fig. 10b (Fig. 10c). The coverage of Doppler radar data in the real TC is not as complete as that in the analytic TCs. Note that HVVP cannot perform well with a large data gap (e.g., large gap of Doppler velocity data south of KBRO as shown in Fig. 10c), which will affect the accuracy of retrieved 16 variables in (7) and further degrade the accuracy of $V_{M\perp}$.

At 2357 UTC, circulation center of Bret is located to the south of KCRP, the coordinate needs a clockwise rotation first, from the true north to the azimuthal angle of the center for later MGBVTD analysis. The circulation center is identified by the ‘‘Simplex’’ algorithm (Lee and Marks 2000). Table 5 shows the sensitivity of the MGBVTD retrievals using KCRP data with respect to different Par at 2 km height where Par is set from 0.3 to 0.7 similar to GM2. The final $V_{M\perp}$ is chosen from the ‘‘optimal’’ results when the RMSE for MGBVTD-retrieved V_{T0} profile to the Rankine profile with the fitted X_T is minimized. The STD of $V_{M\perp}$ for different values of Par is 1.6, larger than that in GM2 (Table 4), but still within 2.0 m s^{-1} . The RMSE for MGBVTD-retrieved V_{T0} profile increases when Par increases, indicating a degradation of the retrieved $V_{M\perp}$ due to the increasing importance of the deformation with increasing Par (i.e., getting close to the eyewall). The retrieved mean STD of $V_{M\perp}$ for KBRO is 4.6 m s^{-1} (not shown) which is more than ten times of that in GM2. This discrepancy is most likely a result from the large gaps in the KBRO data affecting the accuracy of the HVVP analyses. Therefore, the mean wind retrieved from KCRP will be used for KBRO analyses in this study.

The vertical profile of mean wind over KCRP experiences anti-cyclonic shear above 2 km altitude (Fig. 11a). To test the validity of retrieved mean wind, the original GBVTD axisymmetric tangential wind profiles and their corresponding counterparts with the correction of $V_{M\perp}$ by MGBVTD for two radars at 2 km altitude are shown in Fig. 11b. Before the correction, the difference of tangential wind for KCRP and KBRO at R_{\max} is about 3 m s^{-1} and it is larger at farther radius. This can be understood since the difference of the radar-viewing angle from the two radar sites toward the TC center is nearly 180° and the effect of $V_{M\perp}$ on the retrieved axisymmetric tangential wind as shown in (1) is in opposite sign. After the cor-

rection with $V_{M\perp}$ from either MGBVTD, the profiles for two radars are nearly coincident which hints the accuracy of retrieved $V_{M\perp}$. Similarly, the axisymmetric tangential wind profiles for KCRP and KBRO at 3 km altitude are also shown in Fig. 11c, in which the mean difference of amplitude between KCRP and KBRO has dropped from 5.28 m s^{-1} (GBVTD) to 1.63 m s^{-1} (MGBVTD). To quantitatively evaluate the accuracy of MGBVTD-retrieved $V_{M\perp}$, the EGBVTD-retrieved mean wind vector is projected onto the cross-beam direction of both KBRO and KCRP for comparison (Table 6). The MGBVTD-retrieved $V_{M\perp}$ proves to be reliable since it is only 1 m s^{-1} (2 m s^{-1}) larger than its counterpart of EGBVTD at 2 km (3 km) altitude. Meanwhile, the profiles with the correction of EGBVTD-finding cross-beam component for two radars show consistent results with those from MGBVTD (Fig. 11b, 11c).

Similar to the idealized case, the retrieved total winds from GBVTD and MGBVTD are also shown for comparison in Fig. 12. Without retrieving $V_{M\perp}$, the GBVTD-retrieved total winds at 2 km height from KCRP and KBRO are shown in Figs. 12a and 12b. The total wind pattern for KCRP indicates a clearly wavenumber 1 structure while a more asymmetric structure for KBRO. In addition, magnitude of the total wind for KBRO is generally much smaller than that for KCRP. The difference is about 5 m s^{-1} in the southeast of RMW. When including the retrieved $V_{M\perp}$, MGBVTD-retrieved total winds for both KCRP and KBRO shows a consistent wavenumber 1 structure whose maxima winds are greater than 56 m s^{-1} and located in the northwest quadrant (as shown in Figs. 12c, 12d). To investigate how the large data gaps can affect the accuracy of MGBVTD, the total winds retrieved from KBRO data using MGBVTD-retrieved $V_{M\perp}$ from KBRO data is shown in Fig. 12e. As the $V_{M\perp}$ derived from KBRO data is nearly 6 m s^{-1} larger than that of EGBVTD, there is a distinct overestimation (Fig. 12e) in the wind magnitude at the northern part of TC, as compared to Fig. 12d. This proves the aforementioned fact that the large data gap could degrade the accuracy of MGBVTD-retrieved $V_{M\perp}$.

To further quantitatively assess the performance of GBVTD and MGBVTD, the corresponding RMSE (CC) of the retrieved total winds from the two methods (Table 7) are 6.3 (0.91) and 2.0 (0.96), respectively. Clearly, MGBVTD retrieves better TC circulation, a clear advantage and necessity to include $V_{M\perp}$ information in deducing accurate TC circulation. We also applied the MGBVTD to other heights, and MGBVTD can still obtain a better TC circulation than GBVTD can. For example, the RMSE (CC) of the retrieved total winds from GBVTD and MGBVTD at 3 km height are 6.1 (0.90) and 2.0 (0.98) (not shown).

5. Summary and discussion

In this paper, the Modified GBVTD (MGBVTD) method is developed based on the GBVTD (Lee et al. 1999) and HVVP (Harasti et al. 2003) techniques. The individual weakness inherited in GBVTD and HVVP is well known. GBVTD can retrieve reasonable TC circulations but is hindered by its inability to retrieve $V_{M\perp}$. HVVP is designed to deduce $V_{M\perp}$ but needs to use an empirical Rankine profile. By combining GBVTD and HVVP algorithms, MGBVTD retains the strength in both algorithms but avoids their weakness. The GBVTD-retrieved TC circulation can be used to anchor the TC wind profile for HVVP to deduce $V_{M\perp}$ and then be included in the GBVTD analysis to reduce the biases in the retrieved TC circulation. A better TC circulation can be obtained via an iterative process in MGBVTD.

When tested with a series of analytic TC datasets, the accuracy of MGBVTD-retrieved $V_{M\perp}$ from the true value is within 1 m s^{-1} ($\sim 10\%$) in most cases and the retrieved wind struc-

ture is close to the given one after the correction with $V_{M\perp}$. In addition, the sensitivities of MGBVTD to several parameters are examined using analytical TCs. It has been demonstrated that the MGBVTD algorithm is not sensitive to the mean wind vector (direction and magnitude), the TC axisymmetric wind structure modeled by the modified Rankine-combined vortex (i.e., X_T), or the asymmetry of the TC. MGBVTD is, however, sensitive to the size of the HVVP analysis domain especially when it includes a portion of eyewall circulation where deformation is significant.

When applied to Hurricane Bret, MGBVTD also shows its ability to retrieve a more consistent TC structures when using data from KBRO and KCRP than the GBVTD-retrieved structures because of its ability to deduce accurate $V_{M\perp}$. The closeness of the individually retrieved axisymmetric winds at constant heights from KCRP and KBRO demonstrates the strength of the MGBVTD technique over the GBVTD technique and its potential to be included in real-time TC wind retrieval packages like VORTRAC and for research use. Note that GBVTD has been also successfully applied to retrieving tornado wind field in recent years (Lee and Wurman, 2005; Tanamachi et al. 2007). It is promising to apply MGBVTD in tornado research in the future considering its advantage over GBVTD.

The uncertainties of MGBVTD method may result from several factors that need to be noted. The first one is the deviation of modified Rankine-combined Vortex from real TCs. However, this may be a secondary effect because the modified Rankine-combined vortex approximation is adequate to represent the major circulation characteristics of real TCs. Second, data coverage (e.g., missing data between TC rainbands or in weaker TCs) may contain large gaps as shown in the KBRO data in Hurricane Bret, which can pose great challenge for HVVP to find accurate mean wind information. Under this circumstance, it would be better to verify MGBVTD-estimated mean wind for that radar with the mean wind estimated from other sources, if possible. Finally, the asymmetric radial flow is unresolved in MGBVTD and is aliased into the tangential wind and along-beam mean wind. As shown in Eqs.(1), when the significant wavenumber 2 radial wind exists, the retrieved $V_{M\perp}$ can contain large error. In this situation, some extra wind measurements are required to retrieve the asymmetric radial flow.

Acknowledgments. This work was primarily supported by the Social Common wealth Research Program (GYHY201006007), National Fundamental Research 973 Program of China (2013CB430101), and the National Natural Science Foundation of China (grants 40975011, 41275031 and 40921160381).

References

- Browning, K. A., and R. Wexler, 1968: The determination of kinematic properties of a wind field using Doppler radar. *J. Appl. Meteor.*, **7**, 105-113.
- Donaldson, R. J. Jr., 1991: A proposed technique for diagnosis by radar of hurricane structure. *J. Appl. Meteor.*, **30**, 1636-1645.
- Donaldson, R. J. Jr., and F. I. Harris, 1989: Estimation by Doppler radar of curvature, diffluence, and shear in cyclonic flow. *J. Atmos. Oceanic Technol.*, **6**, 26-35.
- Harasti, P. R., and R. List, 2001: The hurricane-customized extension of the VAD (HEVAD) method: wind field estimation in the planetary boundary layer of hurricanes. Preprints: *30th Conf on Radar Meteorology*, Munich, Germany, Amer. Meteor. Soc., 463-465.
- Harasti, P. R., 2003: The hurricane volume velocity processing method. Preprints, *31st Conf. on Radar Meteorology*, Seattle, WA, Amer. Meteor. Soc., 1008-1011.

- Harasti, P.R., and R. List, 2005: Principal Component Analysis of Doppler Radar Data. Part I: Geometric Connections between Eigenvectors and the Core Region of Atmospheric Vortices. *J. Atmos. Sci.*, **62**, 4027–4042.
- Jou, B. J. D., W. C. Lee, S. P. Liu, and Y. C. Kao, 2008: Generalized VTD retrieval of atmospheric vortex kinematic structure. Part I: Formulation and error analysis. *Mon. Wea. Rev.*, **136**, 995-1012.
- Koscielny, A. J., R. J. Doviak, and R. Rabin, 1982: Statistical considerations in the estimation of divergence from single-Doppler radar and application to prestorm boundary-layer observations. *J. Appl. Meteor.*, **21**, 197–210.
- Lee, W.-C., B. J.-D. Jou, P.-L. Chang, and S.-M. Deng, 1999: Tropical Cyclone Kinematic Structure Retrieved from Single-Doppler Radar Observations. Part I: Interpretation of Doppler Velocity Patterns and the GBVTD Technique. *Mon. Wea. Rev.*, **127**, 2419-2439.
- Lee, W. C. and F. D. Marks, 2000: Tropical cyclone kinematic structure retrieved from single-Doppler radar observations. Part II: The GBVTD-simplex center finding algorithm. *Mon. Wea. Rev.*, **128**, 1925-1936.
- Lee, W.-C., B. J. D. Jou, and F. D. Marks Jr, 2000: Tropical Cyclone Kinematic Structure Retrieved from Single-Doppler Radar Observations. Part III: Evolution and Structures of Typhoon Alex (1987). *Mon. Wea. Rev.*, **128**, 3982-4001.
- Lee, W.-C., and J. Wurman, 2005: Diagnosed Three-Dimensional Axisymmetric Structure of the Mulhall Tornado on 3 May 1999. *J. Atmos. Sci.*, **62**, 2373-2393.
- Lee, W. C. and M. M. Bell, 2007: Rapid intensification, eyewall contraction, and breakdown of Hurricane Charley (2004) near landfall. *Geophys. Res. Lett.*, **34**, L02802, doi:10.1029/2006GL027889.
- Liou, Y. C., T. C. C. Wang, W. C. Lee, and Y. J. Chang, 2006: The retrieval of asymmetric tropical cyclone structures using Doppler radar simulations and observations with the extended GBVTD technique. *Mon. Wea. Rev.*, **134**, 1140-1160.
- Mallen, K. J., M. T. Montgomery, and B. Wang, 2005: Reexamining the near-core radial structure of the tropical cyclone primary circulation: Implications for vortex resiliency. *J. Atmos. Sci.*, **62**, 408–425.
- Roux, F. and F. D. Marks, 1996: Extended velocity track display (EVTD): An improved processing method for Doppler radar observations of tropical cyclones. *J. Atmos. Oceanic Technol.*, **13**, 875-899.
- Tanamachi, R. L., H. B. Bluestein, W.-C. Lee, M. Bell, and A. Pazmany, 2007: Ground-Based Velocity Track Display (GBVTD) Analysis of W-Band Doppler Radar Data in a Tornado near Stockton, Kansas, on 15 May 1999. *Mon. Wea. Rev.*, **135**, 783-800.
- Tuttle J. D. and R. Gall, 1999: A single-radar technique for estimating the winds in tropical cyclones. *Bull. Amer. Meteor. Soc.*, **80**, 653–668.
- Wang, M. J., K. Zhao, W. C. Lee, B. J. D. Jou, and M. Xue, 2012: Retrieval of tropical cyclone primary circulation from aliased velocities measured by single Doppler radar – The Gradient Velocity Track Display (GrVTD) Technique, *J. Atmos. Oceanic Technol.*, **29**, 1026–1041.
- Weatherford, C. L., 1989: The structural evolution of typhoons. Dept. of Atmospheric Sciences Paper 446, Colorado State University, 198 pp.
- Willoughby, H. E., 1995: Mature structure and evolution. WMO/TD No. 693 – Global Perspectives on Tropical Cyclones, R. L. Elsberry, Ed., WMO, Geneva, 21-62.
- Zhao, K., Lee W. C., and Jou B. J.-D. Single Doppler Radar Observation of the Concentric Eyewall in Typhoon Saomai (2006) near Landfall, 2006, *Geophys. Res. Lett.*, 2008, doi: 10.1029/2007GL032773.

Zhu, W. J., K. Zhao, X. M. Chen and M. J. Wang, 2010: Separation of the environmental wind and typhoon by Extended-hurricane volume velocity processing method. *Journal of Nanjing University (Natural Science Edition)*, **3**, 243-253. (in Chinese).

Table 1: A list of acronyms used in this paper.

<i>Acronyms</i>	<i>Denotation</i>
VTD	Velocity Track Display
GVTD	General VTD
GBVTD	Ground-based VTD
GB-EVTD	Ground-based Extended VTD
EGBVTD	Extended GBVTD
GrVTD	Gradient VTD
MGBVTD	Modified GBVTD
HVVP	Hurricane Volume Velocity Processing
EHVVP	Extended HVVP
RMSE	Root Mean Square Error
STD	Standard Deviation
CC	Correlation Coefficient
GM1~3	Axisymmetric idealized tests in Part 3
AV1~3	Asymmetric idealized tests in Part 3
GC	Center sensitivity idealized test in Part 3
PPI	Plan Position Indicator
CAPPI	Constant-altitude PPI

Table 2: The definitions of the symbols used in this paper.

<i>Symbol</i>	<i>Definition</i>
V_M	Mean wind
$V_{M\perp}(V_{M\parallel})$	Cross-beam (along beam) component of mean wind
$V_{M\perp\text{guess}}$	Guessed value of $V_{M\perp}$ in each iterative step of MGBVTD
$V_{M\perp\text{ret}}$	Retrieved value of $V_{M\perp}$ in each iterative step of MGBVTD
V_{T0}	Axisymmetric tangential wind
V_T	Total tangential wind (including asymmetry)
V_{R0}	Axisymmetric radial wind
V_R	Total radial wind (including asymmetry)
V_d	Doppler velocity datum
θ_T	Angle for the circulation center relative to radar
θ_M	Direction of mean wind
R_{max}	Radius of maximum wind
$R(R_T)$	Range from the circulation center to GBVTD ring (radar)
R_a	Radius of HVVP analysis domain centered at the radar
Par	$Par = R_a / (R_T - R_{\text{max}})$
ρ	$\rho = R_{\text{max}} / R_T$
$A_n(\delta_n)$	Magnitude (phase) of the asymmetric tangential wind for angular wavenumber n
$\lambda_n(\sigma_n)$	Magnitude (phase) of the asymmetric radial wind for angular wavenumber n
φ	Elevation of radar beam
α	Angles measured anticlockwise from the north to the data position on GBVTD ring
γ	Angle for data position on GBVTD ring relative to TC center
z_0	Analytic altitude of HVVP
z	Altitude at each Doppler velocity datum
$u_0(v_0)$	Total wind component in the cross-beam (along-beam) direction
$P_m(K_m)$	Coefficient matrix (predicted parameters) of HVVP

Table 3: Summary of the sensitivity tests on MGBVTD. Two test series were conducted to evaluate the sensitivity on direction of mean wind (GM1), Rankine X_T (GM2), radius of maximum wind (GM3) and the asymmetry (AV), as well as a misplaced center (GC).

Test series	Parameters
GM1	$V_M = 10.0ms^{-1}, \theta_M = 0 \sim 360^\circ$
GM2	$V_M = 10.0ms^{-1}, \theta_M = 180^\circ, X_T = 0.3 \sim 1.0$
GM3	$V_M = 10.0ms^{-1}, \theta_M = 180^\circ, R_{max} = (0.1 \sim 0.7) * 80km$
AV1	$V_M = 10.0ms^{-1}, \theta_M = 180^\circ, \delta_1 = 0 \sim 360^\circ$
AV2	$V_M = 10.0ms^{-1}, \theta_M = 180^\circ, \delta_2 = 0 \sim 360^\circ$
AV3	$V_M = 10.0ms^{-1}, \theta_M = 180^\circ, \delta_3 = 0 \sim 360^\circ$
GC	$\Delta X = -3km \sim 3km, \Delta Y = -3km \sim 3km$

Table 4: STD information for MGBVTD-retrieved $V_{M\perp}$ of different X_T in GM2.

X_T	0.3	0.4	0.5	0.6	0.7	0.8	0.9	1
$V_{M\perp}$ STD	0.4	0.3	0.3	0.2	0.1	0.1	0	0

Table 5: Mean Wind Information at 2KM Height from KCRP for each Par and corresponding STD for cross-beam component of mean wind. Boldface indicates final result of MGBVTD analysis. $(V_{T0})_{RMSE}$ denotes the RMSE of MGBVTD-retrieved V_{T0} profile to the Rankine profile corresponding to the fitted X_T .

Height	PAR	X_T	$(V_{M\perp}, V_{M\parallel})$	(U, V)	$(V_{T0})_{RMSE}$
2KM	0.3	0.39	(7.2, 2.6)	(-6.8, -3.5)	0.028
	0.4	0.37	(5.7, 2.6)	(-5.3, -3.3)	0.037
	0.5	0.35	(3.9, 2.6)	(-3.5, -3.1)	0.054
	0.6	0.34	(3.5, 2.6)	(-3.1, -3.0)	0.059
	0.7	0.34	(3.5, 2.6)	(-3.1, -3.0)	0.059
$V_{M\perp}$ STD			1.6		

Table 6: MGBVTD- and EGBVTD-retrieved $V_{M\perp}$ Information at 2 km and 3 km altitude for Hurricane Bret.

Height (km)	Radar	Method	
		MGBVTD	EGBVTD
2	KCRP	7.2	6.2
	KBRO	-6.7	-7.7
3	KCRP	9.5	6.6
	KBRO	-9.3	-7.9

Table 7: RMSE and CC of GBVTD- and MGBVTD- retrieved total winds at 2 km altitude for Hurricane Bret.

Radar	Method	
	GBVTD	MGBVTD
RMSE	6.3	2.0
CC	0.91	0.96

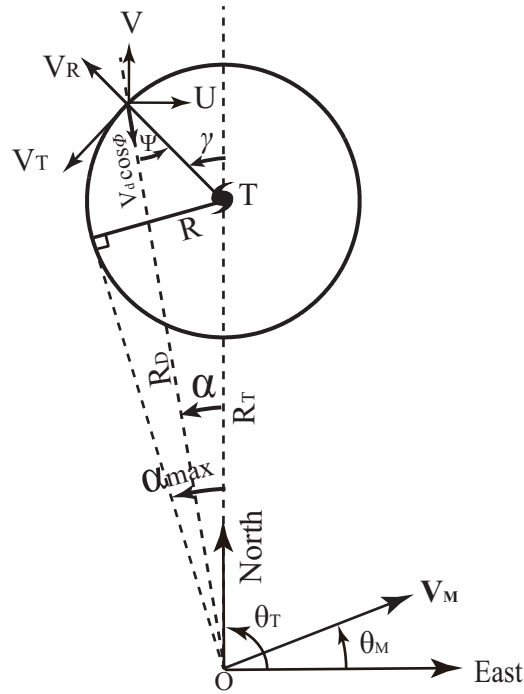


Fig. 1. The MGBVTD geometry and symbols (synthesized from Lee et al. 1999 and Harasti et al. 2003)

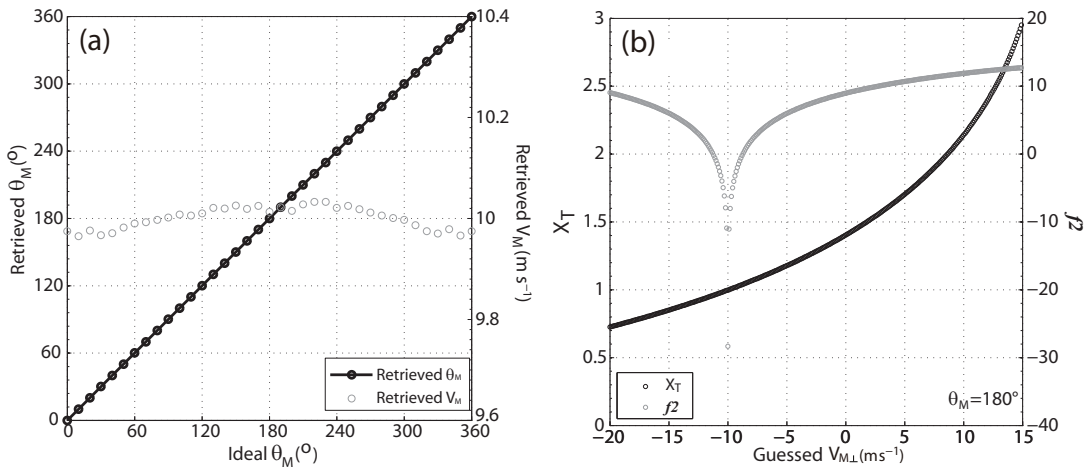


Fig. 2. (a) Retrieved magnitude and direction of mean wind for experiment GM1. (b) Searching process of MGBVTD when there is only easterly mean wind; the gray circle denotes the value of $f2$ as given in Eq. (14) while the black circle is the retrieved X_T .

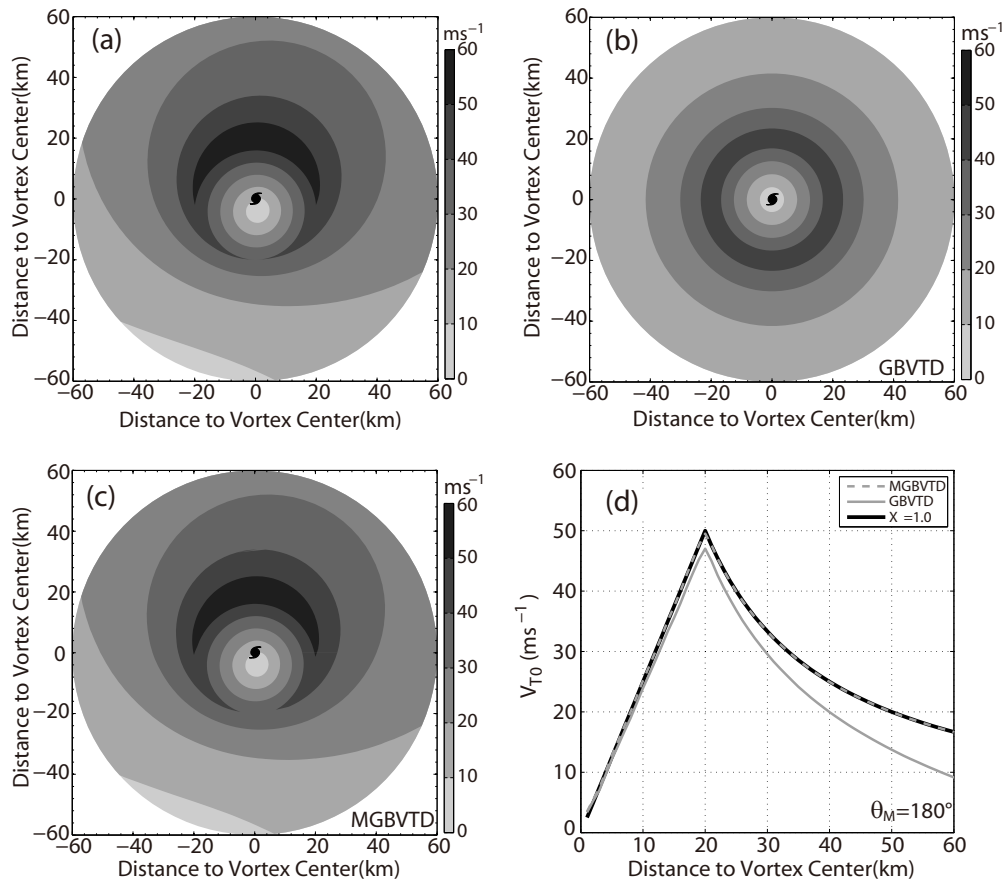


Fig. 3. (a) The analytic total wind field (axisymmetric tangential and radial winds plus an easterly mean wind). GBVTD- and MGBVTD-retrieved total winds are shown in (b), (c), specifically. (d) The axisymmetric tangential wind profile corresponding to image (a) (black line); The gray solid (dash) line denotes the retrieved profile by GBVTD (MGBVTD).

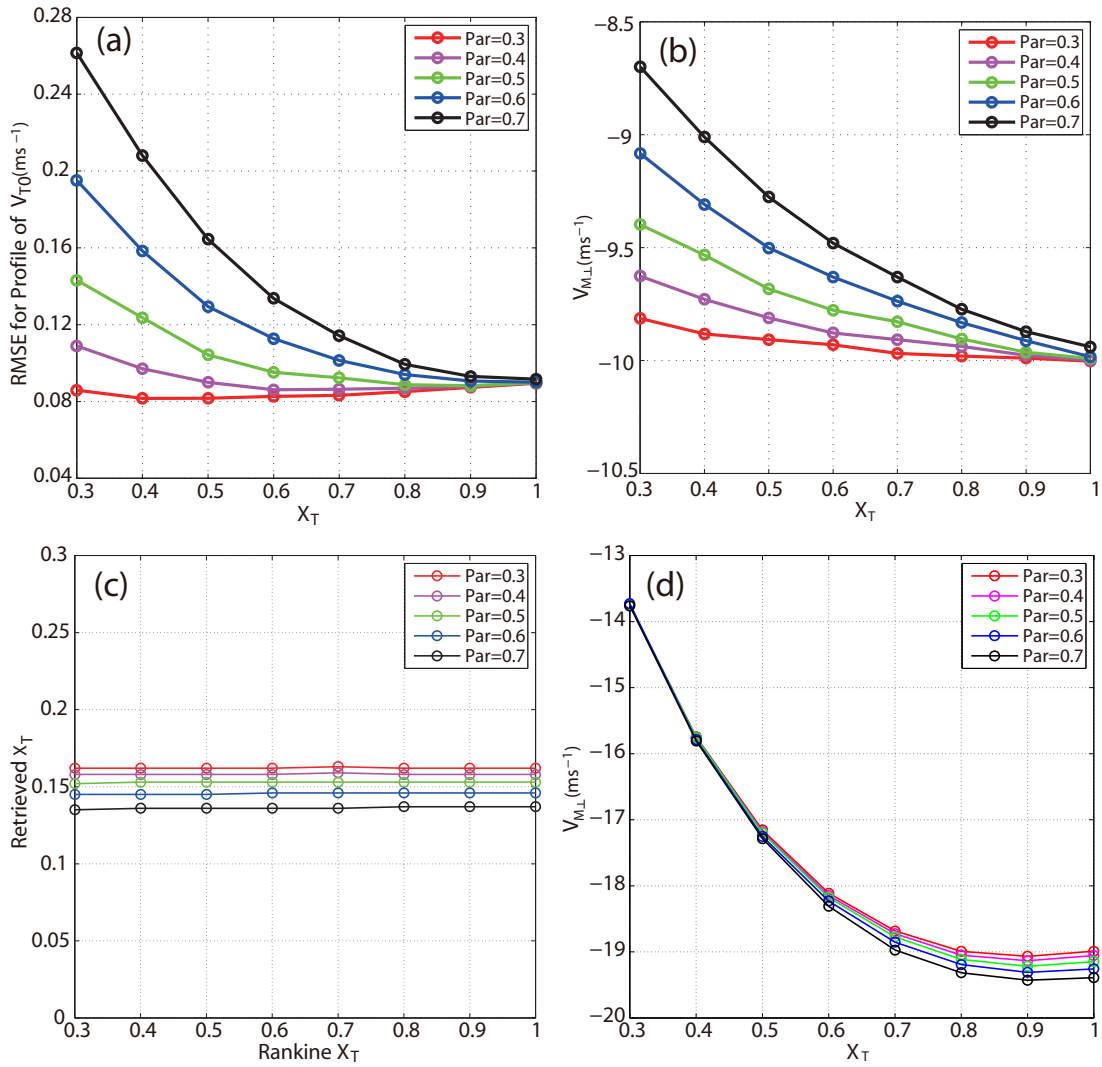


Fig. 4. (a) RMSE for MGBVTD-retrieved axisymmetric tangential wind profile to the corresponding Rankine profile. (b) MGBVTD-retrieved $V_{M\perp}$ for experiment GM2. (c) HVVP-retrieved X_T . (d) Similar to (b), but for HVVP-retrieved $V_{M\perp}$. Different line colors denote different HVVP parameter Par .

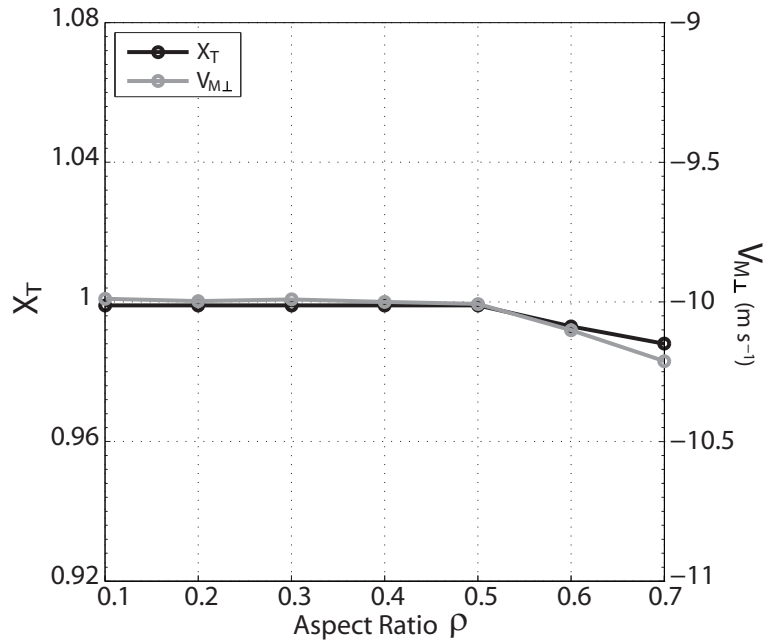


Fig. 5. Retrieved X_T and $V_{M\perp}$ for experiment GM3. The X label ρ is defined as $\rho = R_{\max} / R_T$.

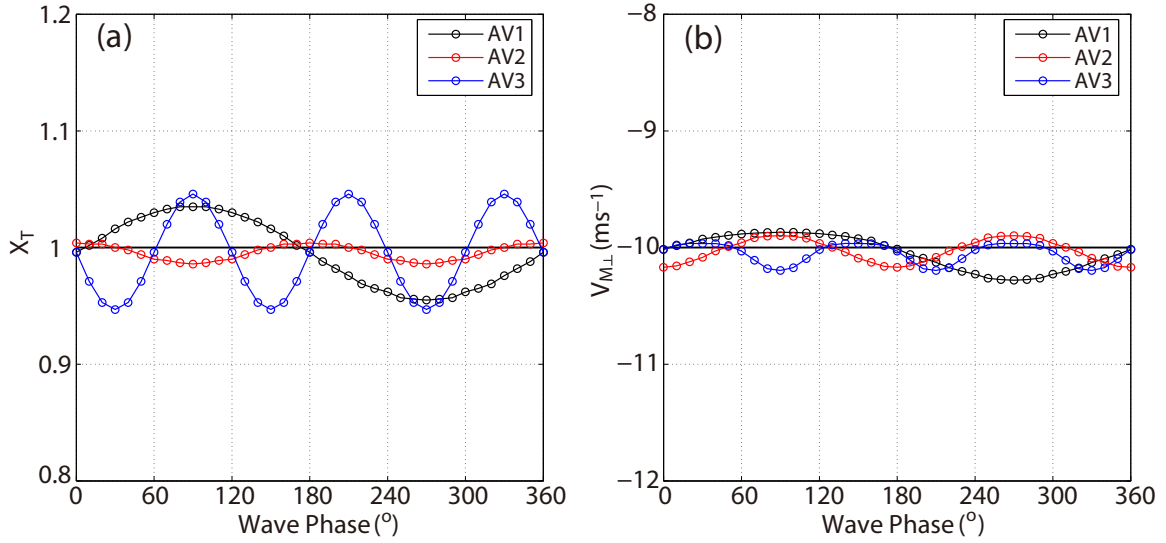


Fig. 6. Retrieved X_T (a) and $V_{M\perp}$ (b) for experiment AV series. The x-axis denotes the phase of asymmetric tangential wind (δ_n).

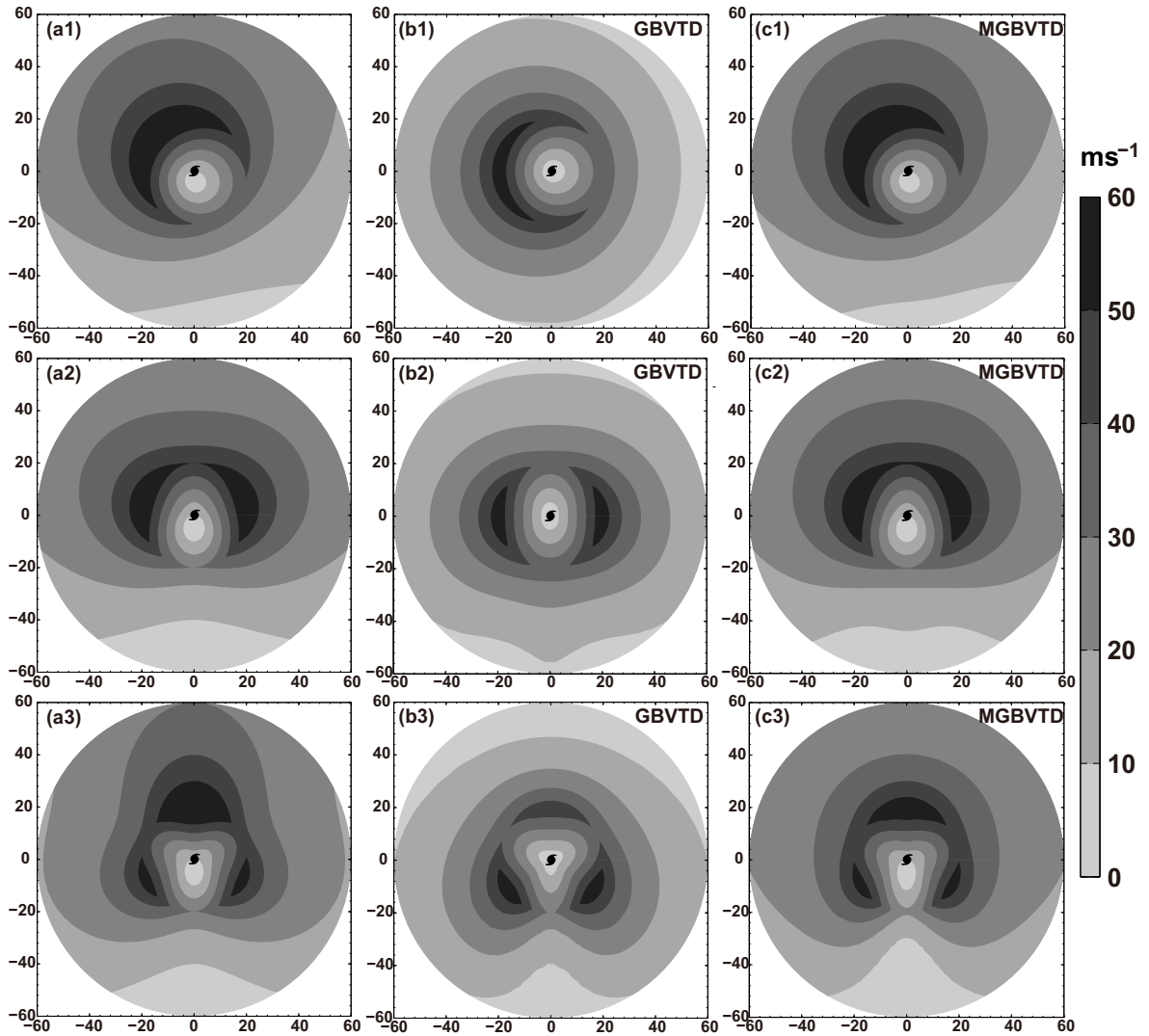


Fig. 7. Comparison of the GBVTD- (2nd column) and MGBVTD- (3rd column) total winds (similar to Fig 1) for experiment series AV1 (1st row), AV2 (2nd row) and AV3 (3rd row), as compared to the simulated total winds (1st column).

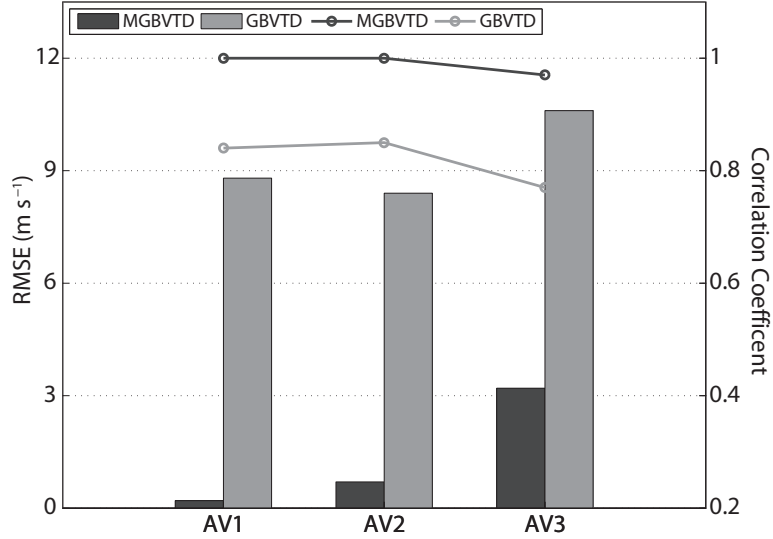


Fig. 8. Comparison of the RMSE and CC of the GBVTD- and MGBVTD-retrieved total winds for AV1~3 tests. The bar denotes RMSE while line denotes CC.

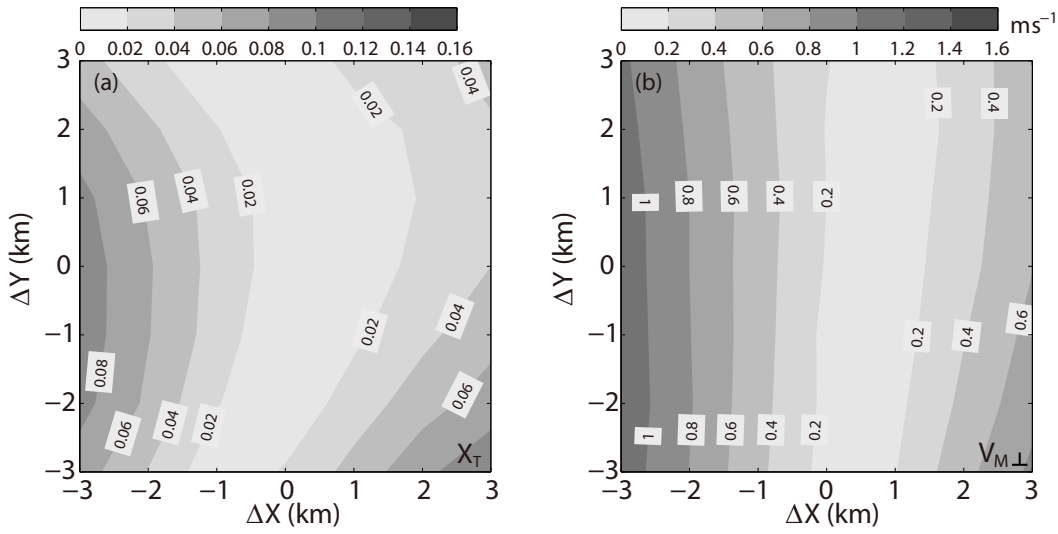


Fig. 9. Retrieval error for X_T (a) and $V_{M\perp}$ (b) in experiment GC. ΔX and ΔY denote the center displacement in X and Y coordinate, respectively.

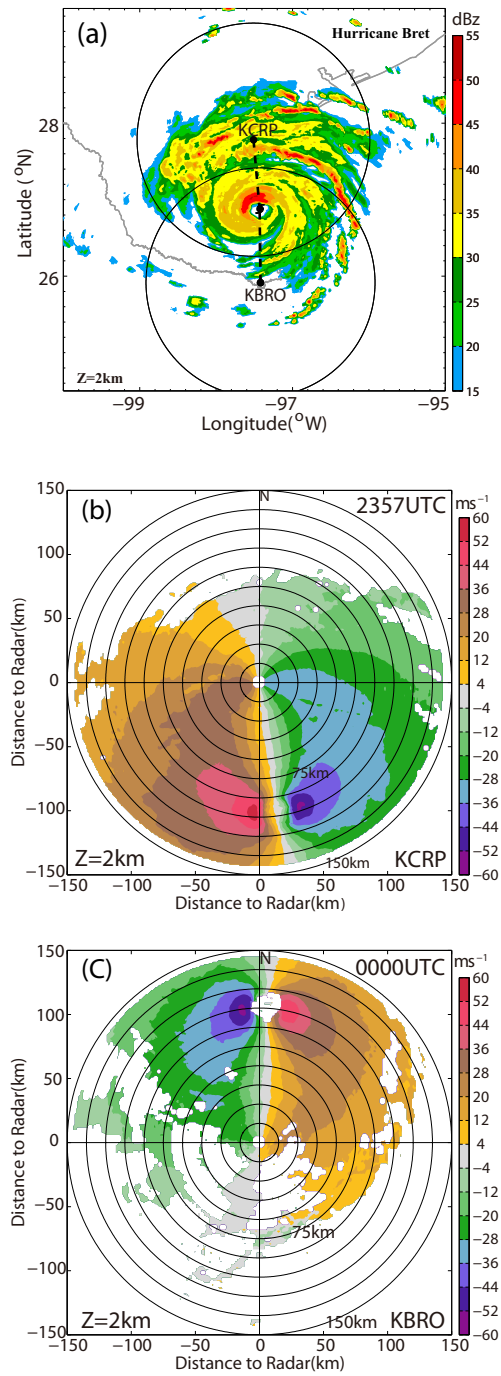


Fig. 10. (a) The dual-Doppler radar mosaic of 2km height at 0000UTC on August 23 1999. Hurricane symbol represents circulation center at that time. The radius of black circles is 150km centered on each Doppler radar. Doppler velocity image of 2km height at (b) 2357 UTC on 22 August from KCRP radar and (c) 0000 UTC on 23 August from KBRO radar.

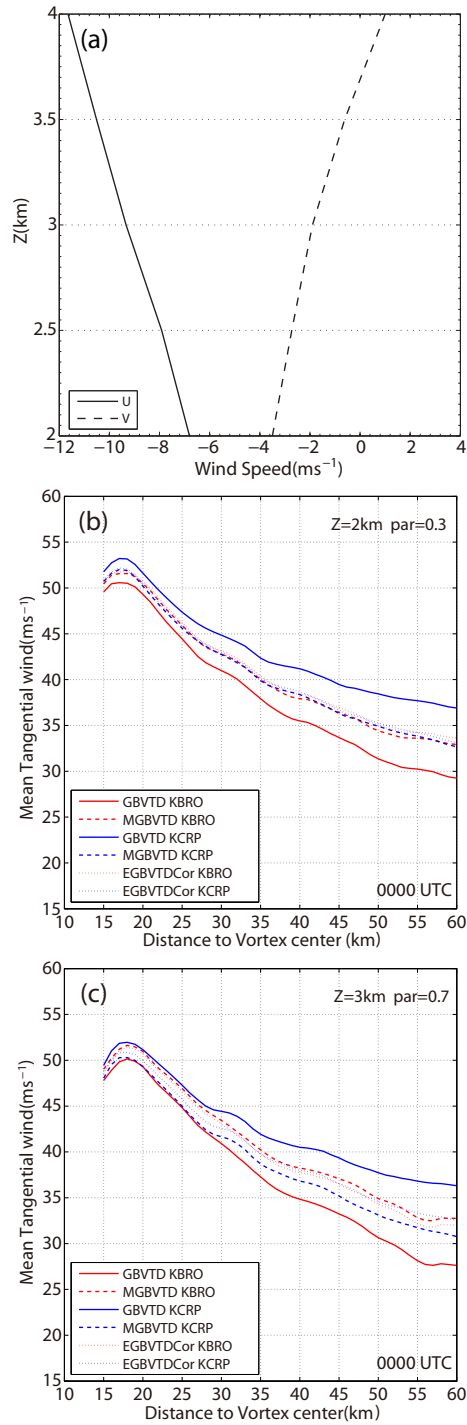


Fig. 11. (a) Vertical profile of mean wind from 2 km to 4km altitude retrieved by MGBVTD; U(V) denotes the direction of east(north). (b) Retrieved mean tangential wind profiles at 2km height by GBVTD (solid lines), with the correction of $V_{M\perp}$ by MGBVTD (dash lines) and by EGBVTD (dot lines). (c) Similar to (b), but for 3km height.

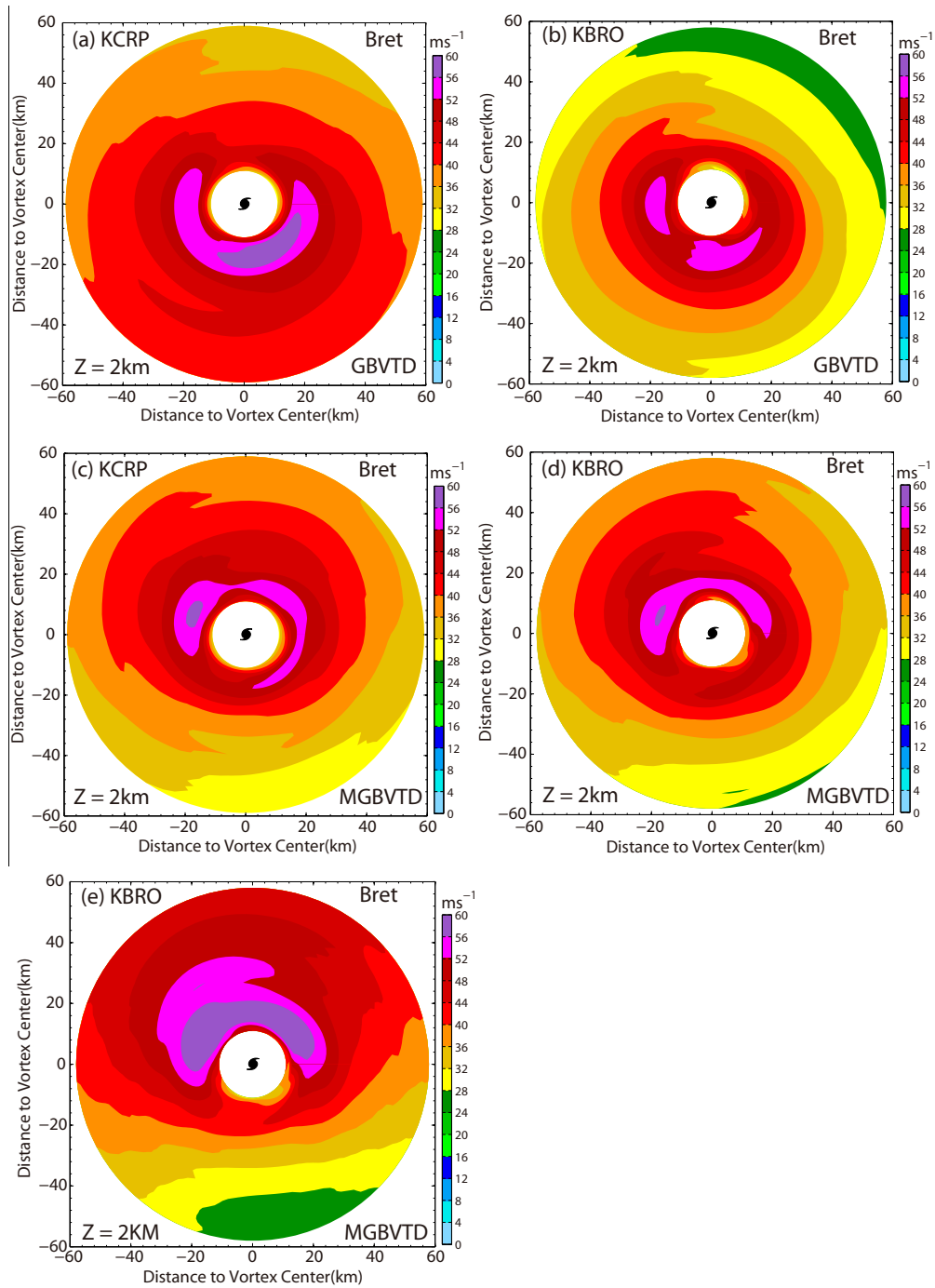


Fig. 12. Ground-relative wind speed for Hurricane Bret at 2-km altitude above sea level (ASL) calculated from the KCRP CAPPI map (left) and KBRO CAPPI map (right), by GBVTD (top row), MGBVTD using KCRP-retrieved mean wind (middle row) as well as MGBVTD using KBRO-retrieved mean wind (e).